



## Oxidation Kinetics of Zr-Nb Alloys in Dry Air in the Temperature Range 723-790 K

S. P. Roy\*, N. K. Gupta, S. K. Mukerjee, S. C. Parida

Product Development Section, Radiochemistry and Isotope Group, Bhabha Atomic Research Centre, Trombay, Mumbai, Maharashtra, India.

Received 08<sup>th</sup> August 2017; Revised 24<sup>th</sup> August 2017; Accepted 26<sup>th</sup> August 2017

### ABSTRACT

The reaction kinetics of three different Zr–Nb alloys with Zr-0.7 wt% Nb, Zr-2.5 wt% Nb, and Zr-5 wt% Nb were investigated using the thermogravimetric technique in the temperature range of 723-790 K. Analysis of the oxidation curves revealed that, at all oxidation temperatures, the reaction follows initially parabolic and then linear oxidation reaction mechanism. The X-ray powder diffraction pattern of the oxidation products revealed the formation of  $ZrO_{0.27}$  and  $Nb_{0.20}Zr_{0.80}O_{2.10}$  at each temperature. The rate constants were evaluated using rate equation and the activation energy by Arrhenius equation in both the parabolic and linear regions of each alloy. The activation energies of Zr-0.7 wt% Nb, Zr-2.5 wt% Nb, and Zr-5 wt% Nb alloys in the parabolic region are 225, 222, and 198 kJ/mol, respectively, whereas in the linear region, the activation energies of the corresponding alloys are 156, 136, and 123 kJ/mol.

**Key words:** Zr–Nb alloys, Oxidation behavior, Activation energy, Thermogravimetric technique.

### 1. INTRODUCTION

Zirconium-niobium alloys are widely used in nuclear industry because of their low neutron absorption and their excellent mechanical and corrosion properties [1-6]. In pressurized heavy water reactors, Zr-2.5 wt% Nb alloy is used as a pressure tube (PT) material in view of its better corrosion resistance, higher mechanical strength, desirable creep resistance, and lower hydrogen pickup over other Zr alloys [7-13]. An addition of small amount of Nb usually leads to the retardation of oxidation of Zr–Nb alloys. It is reported that Zr alloys containing a low Nb content show good corrosion resistance [14,15].

There have been conflicting experimental reports on the effect of Nb on the corrosion kinetics [16-18]. Yilmazbayhan conducted corrosion weight gain measurements on Zr-based alloys with varying Nb content (0.4-2.5 wt% Nb) while keeping other constituents constant but eventually did not identify a clear correlation between Nb content and corrosion kinetics [16]. Similar work by Yueh *et al.* also produced inconclusive results [18]. There are experiments even indicating that Nb-containing alloys exhibit poor corrosion performance. From a study of the effect of the  $\beta$ -phase on corrosion, it has also been reported that corrosion rate of Zr–Nb alloys increases with the formation of the  $\beta$ -Zr phase but decreases with the formation of the  $\beta$ -Nb phase [19-21]. As

such, the corrosion rate of Nb-containing Zr alloys is known to depend on the Nb content in the matrix and the type of  $\beta$ -phases. According to lever rule, the niobium content in these alloys is very low compared to zirconium. Since the mechanical properties of the alloy can be affected by oxygen and moisture at the time of operation of the reactor, it is necessary to investigate the effect of Nb content on the corrosion of Zr–Nb binary alloys for developing advanced nuclear fuel cladding materials with improved corrosion resistance. Studying the corrosion kinetics in various media in different temperature ranges are of importance for a comprehensive understating of the mechanism of oxidation. Most of the literature data on the oxidation behavior of these alloys pertain to moist air/moisture at reactor operating temperatures ( $\sim 573$  K) or very high temperature arising from accident conditions [14-21]. Very limited literature information is available in dry air conditions and in the low or intermediate temperate region. The present study is undertaken to investigate the isothermal oxidation behavior of Zr–Nb alloys in the temperature range of 723-790 K in dry air, though in the actual application, traces of oxygen and moisture would cause the deterioration. This study is essential to derive basic information about the mechanism of air oxidation in the absence of moisture. In the chosen temperature range, the maximum solubility of Nb in the  $\alpha$ -Zr phase [22] is 0.7 wt% beyond which it is in equilibrium with the  $\beta$ -phase.

\*Corresponding Author:  
E-mail: sproy@barc.gov.in

## 2. EXPERIMENTAL PROCEDURES

High-purity niobium and zirconium (each of 99.9 wt pct purity) foils were used to prepare the specimens. Zr–Nb alloys of three different compositions (given in Table 1) were prepared using a commercial arc melting furnace with a water-cooled copper hearth and tungsten electrode. The detailed method of material preparation was reported in an earlier publication [23]. Before melting, the arc melting chamber was evacuated and purged with argon gas several times. To improve the homogeneity, the ingots were arc melted 6 times by turning up-side down after each melting. Each of the cast ingots was wrapped in tantalum foil and annealed in an evacuated sealed quartz tube at 1200 K for 120 h and water quenched to room temperature. The tantalum foil works as a getter for residual oxygen in the quartz ampoule. The annealed samples were cold rolled into sheets of 1-mm thickness. The surfaces of cold-rolled sheets were polished with 600# SiC paper and finely polished with 2- $\mu$ m diamond paste; then, they were thoroughly washed with acetone. The metallic sheets were cut into pieces of  $6 \times 3 \times 1$  mm<sup>3</sup> using a diamond saw cutter for carrying out the oxidation studies.

The phases of the synthesized alloys and their oxidation products were characterized by the X-ray powder diffraction (XRD) method on a STOE X-ray diffractometer (theta-theta geometry) using Ni filter (STOE and Cie GmbH, Germany). The formation of the various phases was established from the comparison of their XRD patterns with the Joint Committee on powder diffraction standards files. The oxidation studies of these alloys were carried out using TG-DTA instrument (Netzsch STA 409 PC, NETZSCH-Geratebau GmbH, Germany).

Before oxidation, the instrument was calibrated for temperature and mass using standard samples. The temperature was calibrated by melting eight different National Institute of Standards and Technology standard samples (In, Sn, Bi, Zn, Al, Ag, Au, and Ni) at a heating rate of 5 K·min<sup>-1</sup> in high-purity argon gas atmosphere with a flow rate of 3.6 dm<sup>3</sup>h<sup>-1</sup>. The observed melting temperatures were compared with

literature values, and the temperature correction factor was determined using the standard software supplied with the instrument and the mass was calibrated by recording the thermal decomposition pattern of CaC<sub>2</sub>O<sub>4</sub>·H<sub>2</sub>O in argon atmosphere at the same heating rate and same flow rate. Isothermal oxidation studies on Zr–Nb alloys were carried out in isothermal mode at four different temperatures, i.e., 723, 748, 773, and 790 K for 45 h in dry air at the same flow rate. All of the oxidation studies were carried out in an alumina crucible, and the oxidation products were identified by the X-ray diffraction method. Morphology of oxide layers was analyzed by taking scanning electron microscope (SEM) images, and the cross-sectional data were obtained by taking EDS spectra.

## 3. RESULTS AND DISCUSSION

### 3.1. Characterization of Alloys

The XRD patterns of the Zr–Nb alloys of three different compositions Zr-0.7 wt% Nb, Zr-2.5 wt% Nb, and Zr-5 wt% Nb along with those for pure Zr and pure Nb are shown in Figure 1. The phase purity of the alloys is confirmed by comparing the XRD patterns with JCPDS (Joint Committee on Powder Diffraction Standards) files (Pure Zr: 01-089-4902, Pure Nb: 00-035-0789, and Zr–Nb alloys: 01-071-9970) [24]. All the three patterns are similar and correspond to ( $\alpha$ -ZrNb) hexagonal phase. Hence, the alloys are considered to be in  $\alpha$ -ZrNb phase.

### 3.2. Oxidation Behavior of Zr–Nb Alloys

The isothermal oxidation behavior of Zr–Nb alloys was investigated in the temperature range of 723–790 K in dry air using thermogravimetric technique for the duration of 45 h at each temperature. The oxidation kinetic curves of the alloys are shown in Figures 2–4, respectively. After oxidation, some spalled-off oxide scales were found in the crucible. The spalled-off oxides obtained from the oxidation reaction of the alloy Zr-0.7 wt% Nb at different oxidation temperatures are taken for XRD study, and the obtained XRD patterns are shown in Figure 5. It is evident from the XRD patterns that the oxidation products are solid solution of oxygen in hcp-Zr(O) and a ternary

**Table 1:** Values of the power exponent ( $n$ ) and the oxidation reaction rate constant ( $k_n$ ) of Zr-0.7 wt.% Nb, Zr-2.5wt.%Nb, and Zr-5wt.%Nb alloys at different temperatures.

Temperature	Zr-0.7 wt% Nb				Zr-2.5 wt% Nb				Zr-5 wt% Nb			
	Parabolic oxidation region		Linear oxidation region		Parabolic oxidation region		Linear oxidation region		Parabolic oxidation region		Linear oxidation region	
T/K	$n$	$\ln k_n$	$n$	$\ln k_n$	$n$	$\ln k_n$	$n$	$\ln k_n$	$n$	$\ln k_n$	$n$	$\ln k_n$
723	1.66	-26.22	1.12	-20.99	1.61	-18.76	1.05	-15.93	1.60	-15.40	0.99	-13.96
748	1.65	-25.02	1.12	-20.24	1.62	-17.73	1.10	-15.36	1.60	-14.46	1.11	-13.49
773	1.65	-23.92	1.11	-19.43	1.61	-16.59	1.12	-14.67	1.61	-13.52	1.12	-12.82
790	1.66	-22.91	1.11	-18.69	1.62	-15.60	1.13	-13.96	1.61	-12.58	1.00	-12.19

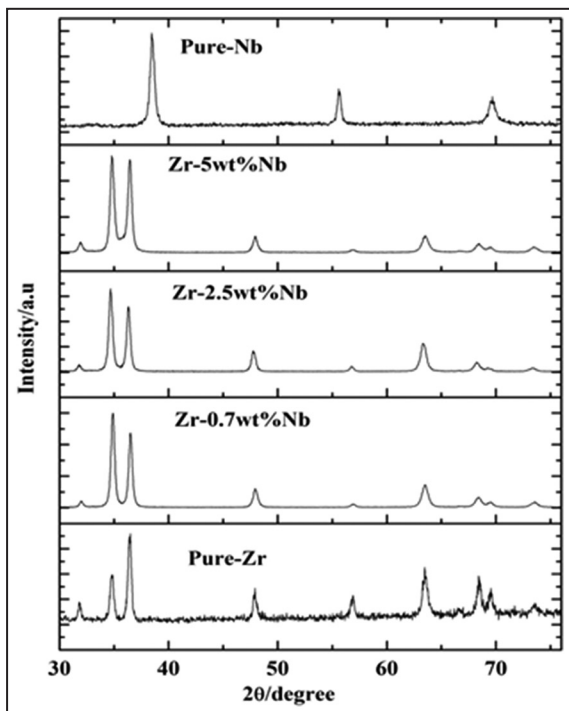


Figure 1: X-ray powder diffraction pattern of Zr–Nb alloys, pure zirconium, and pure niobium.

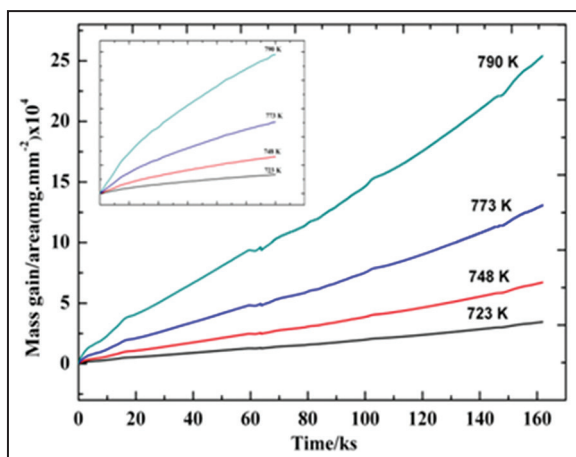


Figure 2: Oxidation kinetic curves of Zr-0.7 wt% Nb.

oxide. The compositions of these two phases closely match with  $ZrO_{0.27}$  (JCPDS file No. 01-089-2340) and  $Nb_{0.20}Zr_{0.80}O_{2.10}$  (JCPDS file No. 00-023-0452) [24]. All the alloys investigated here are zirconium-rich phases. From the phase diagram of Zr–O system [25], it can be predicted that the maximum solubility limit of oxygen in  $\alpha$ -Zr is around 35 at% oxygen at 2338 K. At lower temperatures (~800 K), the solubility of oxygen in  $\alpha$ -Zr is approximately 28-30 at%. Hence, it is expected that in zirconium-rich alloys, the initial oxidation product should be the solution of oxygen in Zr which is confirmed from XRD analysis. However, as the oxidation progresses, the oxygen solubility reaches the terminal limit and a ternary compound close to the stoichiometric compound  $Zr_6Nb_2O_{17}$

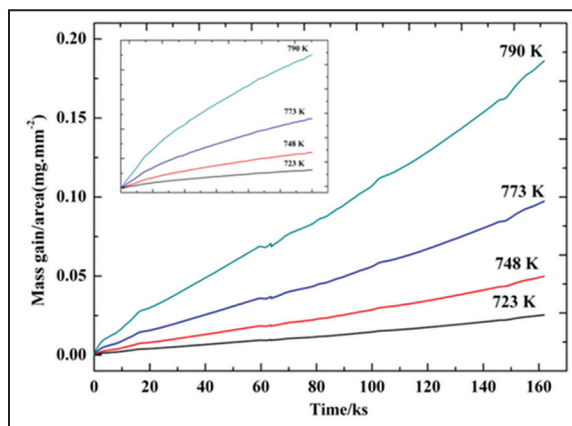


Figure 3: Oxidation kinetic curves of Zr-2.5 wt% Nb.

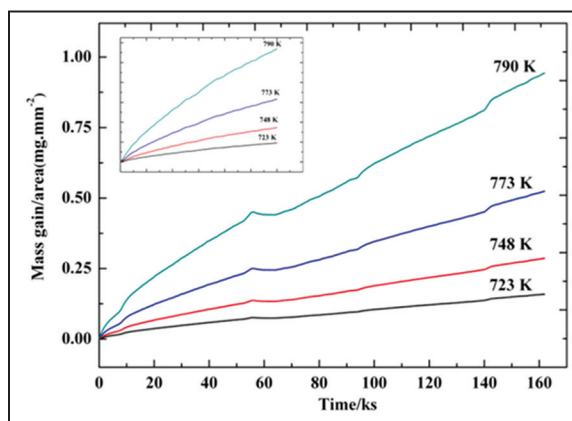
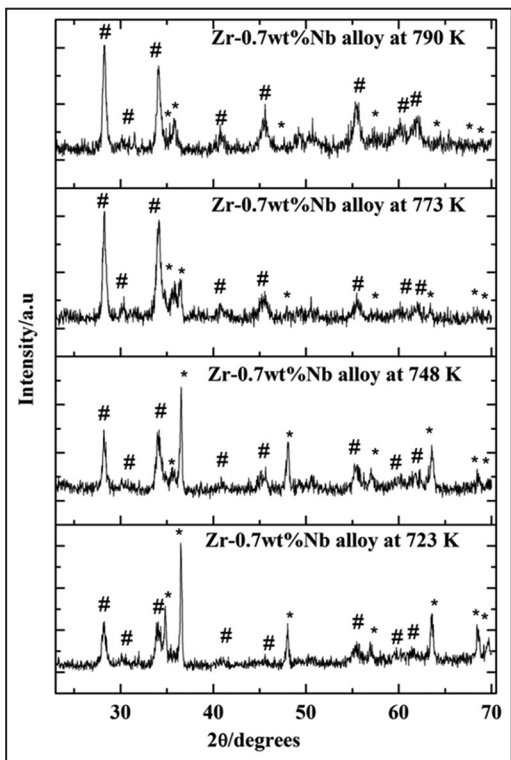


Figure 4: Oxidation kinetic curves of Zr-5 wt% Nb.

( $6ZrO_2.Nb_2O_5$ ) is formed. To confirm the role of nitrogen, a fresh experiment with dry nitrogen gas was carried out at the highest temperature of 790 K for 45 h. The thermogram did not show any weight gain indicating that in the present temperature range of oxidation, nitrogen does not play any role.

The XRD patterns of the oxidation products of Zr-0.7 wt% Nb alloy at different oxidation temperatures as given in Figure 5 show that  $ZrO_{0.27}$  formation decreases, but the formation of  $Nb_{0.20}Zr_{0.80}O_{2.10}$  increases with increase in temperature. Similar patterns were obtained for all the three compositions of the Zr–Nb alloys. Further, the XRD pattern of oxidation of Zr-0.7 wt% Nb, Zr-2.5 wt% Nb, and Zr-5 wt% Nb alloys at 790K given in Figure 6 shows that the formation of  $Nb_{0.20}Zr_{0.80}O_{2.10}$  increases and  $ZrO_{0.27}$  decreases with increasing the niobium content. The same patterns were obtained at all temperatures of these three alloys. The SEM images of Zr-0.7 wt% Nb alloy at 790 K temperature as given in Figure 7a and b show that coarse grained oxides are formed at high temperature which results in cracking of the surface and delamination of oxide layers from the alloy surface which was observed during TG experiments. Similar results were obtained in all the three compositions of Zr–Nb alloys. Further, the EDS



**Figure 5:** X-ray powder diffraction pattern of oxidation of Zr0.7 wt% Nb alloy at different temperatures.  $ZrO_{0.27}(*)$ .  $Nb_{0.20}Zr_{0.80}O_{2.10}(\#)$ .

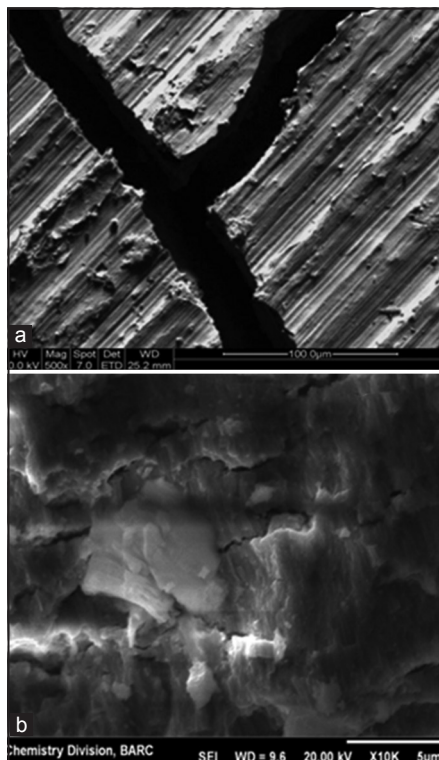


**Figure 7:** (a and b) Scanning electron microscope images of oxidation layer of Zr-0.7 wt% Nb alloy at 790 K.

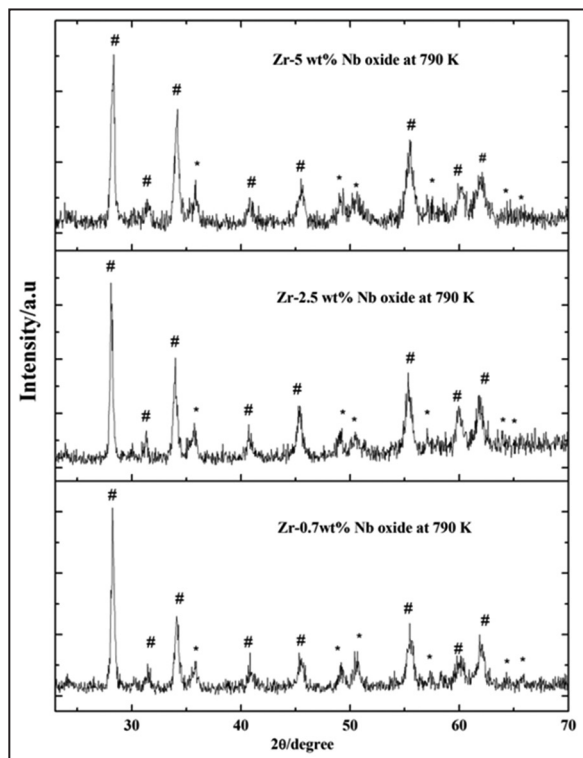
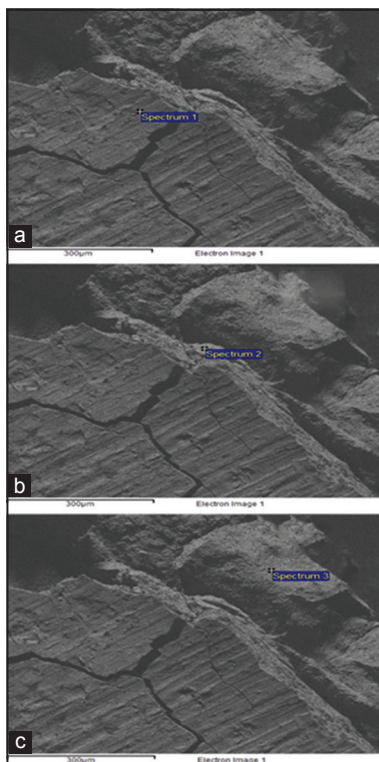


**Figure 6:** X-ray powder diffraction pattern of oxidation of Zr-0.7 wt% Nb, Zr-2.5 wt% Nb, and Zr-5 wt% Nb alloy at 790K.  $ZrO_{0.27}(*)$ .  $Nb_{0.20}Zr_{0.80}O_{2.10}(\#)$ .

analysis of the cross-sections of the specimen was carried out to find the Zr:Nb ratio. It was observed that the Zr:Nb ratio of the surface oxide layer as shown in Figure 8a is 25:1, whereas for the underneath layers as shown in Figure 8b and c, the ratio becomes 17:1. This indicates that Zr gets preferentially oxidized in the beginning and then reacts with Nb to form the ternary oxide.

In all the three alloys, the oxidation reaction initially follows parabolic up to 3600 s and then shifted to linear. The parabolic nature of oxidation kinetics is commonly observed due to the oxygen diffusion through the oxide film. Hence, in this case, the oxygen diffusion through the solid solution hcp-Zr(O) is the cause of parabolic reaction kinetics. During the progress of the oxidation reaction, the formation of the ternary oxide results in cracking of the oxide layer which results in exposing the freshly available reactive surface of the alloy, thereby causing the reaction to follow linear oxidation behavior. The details of calculation of the rate constant and the activation energies were already explained in earlier publication [26]. The rate constant was calculated using the rate equation:  $(\Delta m/a)^n = kt$ , where  $(\Delta m/a)$  ( $mg.mm^{-2}$ ) is the mass gain per unit area,  $n$  is the power exponent,  $k$  ( $mg.mm^{-2}sec^{-1}$ ) is the rate constant, and  $t$  is time in sec. The value of the power



**Figures 8:** (a-c) EDS spectra of oxidation layers of Zr-0.7 wt% Nb alloy at 790 K.

exponent ( $n$ ) and the oxidation reaction rate constant ( $k$ ) of the parabolic and linear regions are summarized in Table 1. The activation energies were calculated using Arrhenius equation:  $k = A \cdot \exp(-E_a/RT)$ , where  $k(\text{mg} \cdot \text{mm}^{-2} \cdot \text{sec}^{-1})$  is the overall oxidation reaction rate constant,  $A(\text{mg} \cdot \text{mm}^{-2} \cdot \text{sec}^{-1})$  is the pre-exponential factor,  $E_a(\text{J} \cdot \text{mol}^{-1})$  is the energy of activation,  $R(\text{JK}^{-1} \cdot \text{mol}^{-1})$  is the universal gas constant, and  $T$  is the temperature in Kelvin. The Arrhenius plots of parabolic and linear rate constants for all the three alloys are shown in Figure 9. The value of activation energy was calculated using slope and intercept of  $\ln k$  versus  $1/T$  in the abovementioned temperature range. The value of activation energy of Zr-0.7 wt% Nb, Zr-2.5 wt% Nb, and Zr-5 wt% Nb alloys in the parabolic region is 225 kJ/mol, 222 kJ/mol, and 198 kJ/mol and in linear region is 156 kJ/mol, 136 kJ/mol, and 123 kJ/mol, respectively.

The oxidation reaction of Zr–Nb alloys at different compositions, different mediums, and different temperature ranges is reported earlier [27-31]. The available data together with the data obtained in the present study are presented in Table 2 for comparison. Elshanshoury *et al.* [27] have observed that the oxidation of Zr-1 wt% Nb followed two stage mechanisms, initially parabolic and then linear in air medium in the temperature range 673-973 K. The same authors have reported that the alloy follows three stage mechanism, initially parabolic, then parabolic or linear

and finally linear in the temperature range 673-973 K. The activation energies obtained are 160.93 kJ/mol in air and 105.75 kJ/mol in steam. Maroto *et al.* [28] have studied the oxidation behavior of Zr-2.5 wt% Nb in steam and observed that the oxidation reaction follows the two-stage mechanism, initially parabolic and then linear in the temperature range of 538-708K and found out the activation energy 131.25 kJ/mol. Bohmert *et al.* [29] have observed that the oxidation kinetics of Zr-1 wt% Nb alloy in steam followed parabolic mechanism in the temperature range of 973-1373K and activation energy was found out to be 85.27 kJ/mol. Park *et al.* [30] have studied the oxidation behavior of Zr-1 wt% Nb alloy in steam and observed that the oxidation followed the parabolic mechanism in the temperature range of 973-1473K and activation energy obtained was 88.61 kJ/mol. Kohli *et al.* [31] have studied the oxidation behavior of Zr-2.5 wt% Nb in  $\text{CO}_2$  medium and observed that the oxidation reaction followed parabolic mechanism in pre-transition region and linear in the post-transition region in the temperature range of 873-1173K. The activation energies obtained are 168.19 kJ/mol and 131.79 kJ/mol in pre-transition and post-transition regions, respectively. They have attributed the lower activation energy for long exposure of time. In the present study, the activation energies were calculated in the parabolic and linear region for oxidation reaction in dry air. The oxidation of pure Zr metal in dry oxygen gas was extensively studied [32-38], and it was observed that the initial stage of oxidation follows parabolic or cubic rate law, and for the long period of time, the oxidation gets accelerated according to the linear rate law [34,36-38]. The oxidation product of pure Zr is  $\text{ZrO}_2$ . Arima *et al.* studied the oxidation kinetics of Zr–Nb alloys with Nb contents of 1.0, 2.5, 4.0, 6.0, and 10.0 wt% in the temperature range of 773-873 K under low oxygen potentials using  $\text{CO-CO}_2$  gas mixtures for a period up to 7 day [39]. They have observed that the oxidation progressed according to cubic law for 1 day for all the alloys, whereas alloys with high Nb content showed accelerated oxidation rate at 873 K for 1 week measurements. XRD analyses of the oxide film showed the presence of both monoclinic and tetragonal zirconia phases. EPMA analysis of the oxide layer showed that  $\alpha\text{-Zr(O)}$  formed at the metal oxide interface, and the thickness of this interface layer is more for Zr-1Nb than for the Zr-10Nb alloy. In another study, Arima *et al.* have investigated the oxidation properties of Zr–Nb alloys with 1-10 wt% Nb content in dry air in the temperature range of 973-1273 K [40]. They have observed that the oxidation kinetics obeyed parabolic rate law. They have observed that, in addition to  $\text{ZrO}_2$ , a ternary oxide of composition  $6\text{ZrO}_2\text{-Nb}_2\text{O}_5$  was formed which is believed to promote the oxidation. Further, the mechanism of the oxidation is related to the lattice structures of underlying metal ( $\alpha\text{-Zr}$  or  $\beta\text{-Zr}$ ) phases. The present investigation shows the formation of  $\alpha\text{-Zr(O)}$  and the ternary oxide close to the

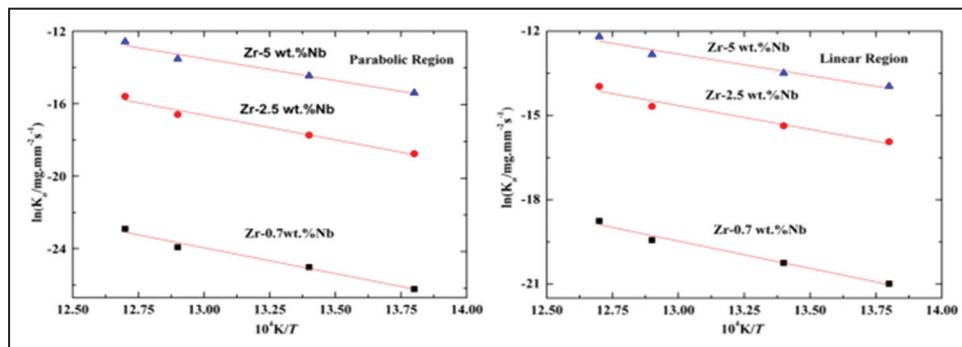


**Figure 9:** Variation of oxidation rate constant of Zr-0.7 wt% Nb, Zr-2.5 wt% Nb, and Zr-5 wt% Nb alloy with respect to reciprocal of temperature.

**Table 2:** Oxidation studies on Zr–Nb alloys at various conditions.

Composition (wt% Nb)	Medium	Temperature range (K)	Rate law	Activation energy (kJ/mol)	Reference
1	Air	673-973	Two-stage initial parabolic then linear	160.93	[27]
1	Steam	673-973	Three-stage initial parabolic, parabolic or linear, and linear	105.75	[27]
2.5	Steam	538-708	Initial parabolic then linear	131.25	[28]
1	Steam	973-1373	Parabolic	85.27	[29]
1	Steam	973-1473	Parabolic	88.61	[30]
2.5	CO <sub>2</sub>	873-1173	Pre-transition region (parabolic)	168.19	[31]
2.5	CO <sub>2</sub>	873-1173	Post-transition (linear)	131.79	[31]
1-10	Dry air	973-1273	Parabolic	150 (≤1073 K)	[40]
				120 (≥1073 K)	
0.7	Dry air	723-790	Initial parabolic than linear	225 <sup>a</sup> , 156 <sup>b</sup>	This study
2.5	Dry air	723-790	Initial parabolic than linear	222 <sup>a</sup> , 136 <sup>b</sup>	This study
5	Dry air	723-790	Initial parabolic than linear	198 <sup>a</sup> , 123 <sup>b</sup>	This study

a: Parabolic, b: Linear

composition Nb<sub>0.20</sub>Zr<sub>0.80</sub>O<sub>2.10</sub> which is in contrary to the reported formation of ZrO<sub>2</sub> and the ternary oxides, and we attribute this due to the low temperature range employed in our investigation.

#### 4. CONCLUSION

The study of oxidation reactions of three Zr–Nb alloys of 0.7, 2.5, and 5 wt% Nb was carried out by isothermal thermogravimetric experiments at four different temperatures of 723, 748, 773, and 790 K for 45 h duration in dry air. The analysis of oxidation curves and XRD analysis of the oxidation products lead to the following conclusions:

- I. Each alloy follows initially parabolic and then linear oxidation behavior.
- II. The oxidation products of each alloy at all four temperatures are ZrO<sub>0.27</sub> and Nb<sub>0.20</sub>Zr<sub>0.80</sub>O<sub>2.10</sub>, respectively.
- III. The oxidation kinetics is governed by the simultaneous formation of both ZrO<sub>0.27</sub> and

Nb<sub>0.20</sub>Zr<sub>0.80</sub>O<sub>2.10</sub>, respectively and thinning of the oxide at the metal oxide/gaseous environment interface by oxide spalling.

- IV. The value of activation energy of Zr-0.7 wt% Nb, Zr-2.5 wt% Nb, and Zr-5 wt% Nb alloys in the parabolic region is 225 kJ/mol, 222 kJ/mol, and 198 kJ/mol and in the linear region is 156 kJ/mol, 136 kJ/mol, and 123 kJ/mol, respectively.

#### 5. REFERENCES

1. C. Ganguly, (2002) Advances in zirconium, *Proceedings of the Symposium Zirconium-2002 BARC, Mumbai, 34(26)*: 1-27.
2. L. Magnus, B. Pierre, (2012) Zirconium in nuclear industry 16<sup>th</sup> International symposium, *Journal of ASTM International Selected Technical Papers STP1529, 5*: 1-14.
3. M. K. Kumar, S. Aggarwal, V. Kain, T. Saario, M. Bojinov, (2010) Effect of dissolved oxygen on oxidation and hydrogen pickup behaviour-zircaloy

- versus Zr-Nb alloys, *Nuclear Engineering and Design*, **240**: 985-994.
4. M. K. Kumar, I. Samajdar, N. Venkataramani, G. K. Dey, R. Tewari, D. Srivastava, S. Banerjee, (2003) Explaining absence of texture development in cold rolled two-phases Zr-2.5wt% Nb alloy, *Acta Materialia*, **51**: 625-640.
  5. R. V. Kulkarni, S. Neogy, B. N. Rath, K. Manikrishna, D. Srivastava, N. Saibaba, I. Samajdar, E. Ramadasan, G. K. Dey, S. Antharaman, (2011) Microstructural and textural evolution in heat treatment Zr-2.5%Nb pressure tube material subjected to dilatometric studies, *Transactions of the Indian Institute of Metals*, **64(4-5)**: 395-399.
  6. M. K. Kumar, C. Vanitha, I. Samajdar, G. K. Dey, R. Tewari, D. Srivastava, S. Banerjee, (2004) Textural and microstructure developments during fabrication of Zr-2.5 wt% Nb pressure tubes, *Journal of Nuclear Materials*, **335**: 48-58.
  7. B. D. C. Bell, S. T. Murphy, R. W. Grimes, M. R. Wenman, (2017) The effect of Nb on the corrosion and hydrogen pick-up of Zr alloys, *Acta Materialia*, **132**: 425-431.
  8. R. K. Kulkarni, K. V. Manikrishna, S. Neogy, D. Srivastava, E. Ramadasan, R. S. Shriwastaw, B. N. Rath, N. Saibaba, S. K. Jha, G. K. Dey, (2014) Mechanical properties of Zr-2.5%Nb pressure tube material subjected to heat treatments in  $\alpha+\beta$  phase field, *Journal of Nuclear Materials*, **451**: 300-312.
  9. G. D. Moan, P. Rudling, (2002) Zirconium in the nuclear industry, *Thirteenth International Symposium STP*, **1423**: 1-399.
  10. C. Vazquez, A. M. Fortis, P. B. Bozzano, (2015) Comparison of mechanical properties of Zr-1% Nb and Zr-2.5% Nb alloys, *Procedia Materials Science*, **8**: 478-485.
  11. R. N. Singh, N. Kumar, R. Kishore, S. Roychaudhury, T. K. Sinha, B. P. Kashyap, (2002) Delayed hydride cracking in Zr-2.5Nb pressure tube material, *Journal of Nuclear Materials*, **304(2-3)**: 189-203.
  12. A. H. Troy, E. K. Michael, (2006) Creep of zirconium and zirconium alloys, *Metallurgical and Materials Transaction A*, **37(8)**: 2389-2396.
  13. S. Kaity, J. Banerjee, M. R. Nair, K. Ravi, S. Dash, T. R. G. Kutty, A. Kumar, R. P. Singh, (2012) Microstructural and thermophysical properties of U-6 wt%Zr alloy for fast reactor application, *Journal of Nuclear Materials*, **427**: 1-11.
  14. H. H. Klepfer, (1963) Zirconium-niobium binary alloys for boiling water reactor service part 1-corrosion resistance, *Journal of Nuclear Materials*, **9**: 65-76.
  15. D. Feron, (2012) *Nuclear Corrosion Science and Engineering*, 1<sup>st</sup> ed. Oxford: Woodhead, p1-1072.
  16. A. Yilmazbayhan, M. G. D. Silva, A. Motta, H. G. Kim, Y. H. Jeong, J. Y. Park, R. Comstock, B. Lai, Z. Cai, (2005) *Proceeding International Conference on Environmental Degradation of Materials in Nuclear Power System-Water Reactor*, Vol. 12. p201-212.
  17. U. Otgonbaatar, W. Ma, M. Youssef, B. Yildiz, (2014) Effect of niobium on the defect chemistry and oxidation kinetics of tetragonal ZrO<sub>2</sub>, *Journal of Physical Chemistry C*, **118(36)**: 20122-20131.
  18. H. K. Yueh, R. L. Kesterson, R. J. Comstock, H. H. Shah, D. J. Colburn, M. Dahlback, L. J. Hallstadius, (2005) Zirconium in nuclear industry, *ASTM International*, **2**: 1-10.
  19. G. P. Sabol, R. J. Comstock, U. P. Nayak, (2000) Zirconium 12<sup>th</sup> nuclear industry, *Twelfth International Symposium ASTM STP*, **1354**: 525-544.
  20. V. F. Urvanic, M. Griffiths, (2000) Microstructural aspects of corrosion and hydrogen ingress in Zr-2.5Nb, *Symposium ASTM STP*, **1354**: 641-657.
  21. Y. H. Jeong, H. G. Kim, T. H. Kim, (2003) Effect of  $\beta$ -phase, precipitate and Nb- concentration in matrix on corrosion and oxide characteristics of Zr-xNb alloys, *Journal of Nuclear Materials*, **317**: 1-12.
  22. J. F. Smith, D. T. Peterson, (1982) Phase diagram features associated with multicritical points in alloy systems. *Bulletin of Alloy Phase Diagrams*, **3(3)**: 287-295.
  23. S. C. Parida, N. K. Gupta, K. Krishnan, G. A. R. Rao, B. K. Sen, (2008) High-temperature oxidation of  $\beta$ -NbTi alloys, *Metallurgical and Materials Transactions A*, **39A**: 2020-2025.
  24. PCPDFWIN, (2001) X-ray data base, JCPDS-International Centre for Diffraction Data Version 2.2.
  25. R. S. Rath, L. S. Coughanour, (1955) Phase equilibrium relations in the systems titania-niobia and zirconia-niobia, *Journal Research of the National Bureau of Standards*, **55**: 209-213.
  26. S. P. Roy, N. K. Gupta, R. A. Jat, S. C. Parida, S. K. Mukerjee, (2016) Oxidation kinetics of UZr<sub>2,3</sub> and U<sub>2</sub>Ti alloy in dry air, *Oxidation of Metals*, **86**: 165-177.
  27. A. Elshanshoury, V. A. Rudenko, M. E. EL-Dahshan, F. H. Hammad, (1969) Kinetics of oxidation of Zr-1%Nb alloy in pressurized steam and air at 400-700°C, *Corrosion Science*, **9**: 217-224.
  28. A. J. G. Maroto, R. Bordoni, M. Villegas, M. A. Blesa, A. M. Olmedo, A. Iglesias, G. Rigoti, (1996) Growth and characterization of oxide layers on zirconium alloys, *National Commission of Atomic Energy, Buenos Aires, Argentina*, **28(11)**: 143-159.
  29. J. Bohmert, M. Dietrich, J. Linek, (1993) Comparative studies on high-temperature corrosion of Zr-1Nb and zircaloy-4, *Nuclear Engineering and Design*, **147**: 53-62.
  30. K. Park, T. Yoo, S. Kim, H. G. Kim, Y. Jeong, K. Kim, (2005) High temperature oxidation of a

- zirconium base alloy in steam, *Transactions of the Korean Nuclear Society*, **34(46)**: 1-10.
31. R. Kohli, (1980) The oxidation kinetics of some zirconium alloys in flowing carbon dioxide at high temperature, *Nuclear Technology*, **47**: 477-484.
  32. R. J. Hussey, W. W. Smeltzer, (1964) The oxidation kinetics of zirconium in the temperature range of 400<sup>0</sup>-600<sup>0</sup>C, *Journal Electrochemical Society*, **111**: 564-568.
  33. T. Smith, (1965) Mechanism of the oxidation of zirconium in oxygen in oxygen and liquid sodium, *Journal Electrochemical Society*, **112**: 39-46.
  34. S. Nomura, C. Akutsu, (1966) Oxidation kinetics and oxide film breakway of zirconium and its alloys at high temperatures, *Electrochemical Technology*, **4**: 93-99.
  35. J. P. Pemsler, (1966) The kinetics and mechanism of oxide film growth of zirconium, *Electrochemical Technology*, **4**: 128-131.
  36. E. Hillner, (1966) The high-temperature oxidation kinetics of zirconium in dry air, *Electrochemical Technology*, **4**: 132-137.
  37. R. A. Ploc, (1979) Breakway oxidation of zirconium at 573 K, *Journal of Nuclear Materials*, **82**: 411-418.
  38. R. A. Ploc, (1980) An electron microscope study of break way oxidation of zirconium at 623 K, *Journal of Nuclear Materials*, **91**: 322-328.
  39. T. Arima, K. Miyata, Y. Inagaki, K. Idemitsu, (2005) Oxidation properties of Zr-Nb alloys at 500-600<sup>0</sup>C under low oxygen potentials, *Corrosion Science*, **47**: 435-446.
  40. T. Arima, K. Miyata, K. Idemitsu, Y. Inagaki, (2009) Oxidation properties of Zr-Nb alloys at 973-1273 K in air, *Progress in Nuclear Energy*, **51**: 307-312.

**\*Bibliographical Sketch**



Shri S.P. Roy, obtained B.Sc chemistry (hons) degree in 1995 from Magadh University. He joined in Fuel Chemistry Division, BARC, Mumbai in February 2002. He obtained his M.Sc. Degree in Chemistry from Mumbai University in 2010, Currently, he is working in Product Development Section, BARC, Mumbai. He has 8 journal publications. He is the member of ITAS, INCAS, ISMAS and NAARI. He has experience in the thermal and oxidation study of the alloys.